MMA Memo 170
System Temperatures, Single Versus Double Sideband Operation, and Optimum Receiver Performance

P. R. Jewell
Joint Astronomy Centre
University Park
660 North A'ohoku Place
Hilo, HI 96720
email: pjewell@jach.hawaii.edu
and
J. G. Mangum
National Radio Astronomy Observatory
949 North Cherry Avenue
Tucson, AZ 85721
email: jmangum@nrao.edu

May 1, 1997

Abstract

This paper discusses the relative observing efficiency of single sideband (SSB) and double sideband (DSB) receiver systems in the presence of atmospheric and antenna losses. We use the antenna parameters currently specified for the MMA antennas and atmospheric opacities appropriate to an excellent site such as the Chilean or Mauna Kea sites under consideration for the MMA. We find that for spectroscopic observations in one sideband, SSB measurements are always more efficient. Below 400 GHz, the observing time advantage is 50-80%. Above 400 GHz, the advantage is over a factor of 2, indicating that SSB-mode observing is more efficient even if spectral lines of interest are present in both sidebands. We discuss the goals for the ultimate, practical receiver performance that we should aim for in the presence of atmospheric and telescope losses. Observing efficiencies are displayed as a

function of frequency using atmospheric opacity models as input. We also develop some analytic expressions for SSB and DSB observing.

1 Introduction

MMA working groups are now considering several issues concerning telescope and receiver design, and the virtues of single sideband (SSB) versus double sideband (DSB) receiver operation. We review here the relationships showing how receiver, atmospheric, and spillover noise affect the effective system temperature. We derive a few results relevant to the single sideband versus double sideband issue, and suggest a goal for the ultimate receiver performance in the presence of atmosphere and spillover losses. In the discussion of each noise and loss term, we present diagrams which characterize what we anticipate the system temperatures will be for a single MMA antenna operating in total power mode.

2 Effective System Temperature

With respect to the signal sideband, the effective system temperature, T_{sys}, referred to a perfect telescope above the earth's atmosphere, is given by (*c.f.* Ulich & Haas 1976; Kutner & Ulich 1981)

$$T_{sys} = \frac{\left(1 + \frac{G_i}{G_s}\right)\left[T_{rx} + T_A(sky)\right]}{\eta_l \eta_{fss} \exp(-A\tau_0)}, \tag{1}$$

where

$\frac{G_i}{G_s}$ is the ratio of the gain response of the image and signal sidebands;

T_{rx} is the receiver noise temperature measured with hot and cold loads (and will generally differ for single and double sideband tunings);

$T_A(sky)$ is the antenna temperature of the sky (see below), and includes contributions from the atmosphere, antenna spillover, and cosmic microwave background;

η_l is the rear spillover, scattering, and ohmic loss efficiency, given by:

$$\eta_l \equiv \frac{G}{4\pi} \iint_{2\pi} P_n(\Omega) d\Omega \tag{2}$$

where $P_n(\Omega)d\Omega$ is the antenna power pattern and G is the maximum antenna gain (*i.e.*, η_l is the fraction of telescope power in the forward hemisphere).

η_{fss} is the forward spillover and scattering efficiency, given by:

$$\eta_{fss} \equiv \frac{\iint_{\Omega_d} P_n(\Omega)d\Omega}{\iint_{2\pi} P_n(\Omega)d\Omega} \tag{3}$$

where Ω_d is a defined diffraction zone.

τ_0 is the zenith optical depth of the atmosphere; and

A is the number of airmasses at the observing elevation (given approximately by $\frac{1}{\sin(elevation)}$).

The T_{sys} definition given in Equation 1 is on the T_R^* scale as defined by Kutner & Ulich (1981). Some observatories prefer the T_A^* scale which differs from T_R^* by the η_{fss} factor. The conclusions of this paper mostly depend on ratios in which η_{fss} divides out, so the difference in definitions is not important.

In Equation 1, the numerator corresponds to the various sources of noise present, whereas the denominator represents the scaling factors that account for signal losses through telescope inefficiencies and atmospheric attenuation. The antenna temperature of the sky is given by the sum of noise contributions due to sky, antenna, and cosmic microwave background emission

$$\begin{aligned} T_A(sky) &= T_{sky}^{cold} + T_{sky}^{hot} + T_{ant} + T_{cmbr} \\ &= \eta_l \eta_{fss} T_M \Big[1 - \exp(-A\tau_0)\Big] + \eta_l \Big(1 - \eta_{fss}\Big)\Big[1 - \exp(-A\tau_0)\Big] T_M \\ &\quad + (1-\eta_l)T_{spill} + \eta_l T_{bg}\exp(-A\tau_0) \\ &= \eta_l T_M \Big[1 - \exp(-A\tau_0)\Big] + (1-\eta_l)T_{spill} + \eta_l T_{bg}\exp(-A\tau_0) \end{aligned} \tag{4}$$

where

T_M is the mean temperature of the atmosphere (given approximately by $\sim 0.95 T_{ambient}$. This quantity is frequency and weather dependent and can be given more accurately by atmospheric models.);

T_{spill} is the effective temperature of the rear spillover (also $\sim 0.95 T_{ambient}$);

T_{bg} is the background temperature (usually taken to be the cosmic background temperature of 2.7 K).

To properly calculate Equations 1 and 4, the temperatures used should be the equivalent Rayleigh-Jeans temperatures of the point on the Planck blackbody curve corresponding to the same frequency.[1] This correction factor is given by (see Ulich & Haas 1976)

$$J(\nu, T) = \frac{\frac{h\nu}{k}}{\exp\left(\frac{h\nu}{kT}\right) - 1}. \tag{5}$$

For simplicity of notation, we will retain the symbol "T" for temperatures, but in calculations T should be replaced by J(ν,T).

Real receivers, whether they are intended to be single or double sideband, have varying ratios of sideband gain $\frac{G_i}{G_s}$, *i.e.* single sideband systems have imperfect rejection so that $\frac{G_i}{G_s} > 0$, while double sideband systems often have slightly unequal gain ratios so that $\frac{G_i}{G_s} \neq 1$. However, these are usually minor effects in terms of system temperature, so we will consider the two cases of principal interest

Single Sideband $\rightarrow \frac{G_i}{G_s} = 0$,

Double Sideband $\rightarrow \frac{G_i}{G_s} = 1$.

Furthermore, we will take[2]

$$T_{rx}(SSB) = 2T_{rx}(DSB) + T_{image}. \tag{6}$$

where T_{image} is the image termination physical temperature, which is, for example, ~ 30 K for the quasi-optical image termination of the 1.3mm dual-channel receiver on the NRAO 12m telescope. For quasi-optical systems the image termination temperature is also increased by optics losses, such as vacuum windows, grids, *etc.* before the beam terminates on an absorber. Thus, the system temperature of a single sideband system is

[1] Note that in MMA Memo 161, Kerr, Feldman, & Pan advocate the use of the Callen & Welton (1951) generalization of the Nyquist theorem for the calculation of noise temperatures. Since the zero-point noise is included in the receiver noise temperature when the receiver noise is measured using the Y-factor method with hot and cold noise temperatures determined with the Planck equation, we will use the Planck formalism in this paper.

[2] With some image rejection systems it is possible to optimize performance for the signal sideband such that $T_{rx}(SSB) < 2T_{rx}(DSB)$, neglecting termination noise.

$$T_{sys}(SSB) = \frac{2T_{rx}(DSB) + T_A(sky) + T_{image}}{\eta_l \eta_{fss} \exp(-A\tau_0)} \tag{7}$$

$$= \frac{2T_{rx}(DSB)}{\eta_l \eta_{fss} \exp(-A\tau_0)} + \frac{T_A(sky) + T_{image}}{\eta_l \eta_{fss} \exp(-A\tau_0)} \tag{8}$$

The SSB system temperature of a double sideband system is

$$T_{sys}(DSB) = \frac{2\Big[T_{rx}(DSB) + T_A(sky)\Big]}{\eta_l \eta_{fss} \exp(-A\tau_0)} \tag{9}$$

$$= T_{sys}(SSB) + \frac{T_A(sky) - T_{image}}{\eta_l \eta_{fss} \exp(-A\tau_0)} \tag{10}$$

The factor

$$\Gamma = \frac{T_A(sky) - T_{image}}{\eta_l \eta_{fss} \exp(-A\tau_0)} \tag{11}$$

is the difference between single and double sideband system temperatures, and can be thought of as the *double sideband penalty.* As is apparent, if the termination temperature of the image sideband, T_{image}, exceeds $T_A(sky)$, the double sideband "penalty" becomes an advantage. The product of the spillover efficiencies, $\eta_l \eta_{fss}$, is an upper limit on the conventional beam efficiency, η_b. Through arrangement of optics and by redirecting spillover between the ground and the sky, one can transfer losses between η_l and η_{fss}. It is most advantageous to maximize η_l since it contributes to both an ambient temperature noise term and a loss factor. η_{fss} contributes only a loss factor and is a simple scaling factor.

3 Single Sideband and Double Sideband Noise Trade-offs: When is DSB More Efficient Than SSB?

With respect to observations in a given sideband, one can usually improve sensitivity by rejecting the image sideband, as indicated in Equation 10 above. Nevertheless, spectral lines of interest are sometimes present in both sidebands. Given that one usually pays a noise penalty by observing in double sideband mode, at what point do we break even if lines of interest can be observed simultaneously in both sidebands? Put another way, when would we be better off from a noise standpoint to make two single sideband observations of the two sidebands rather than one simultaneous observation in double sideband mode? Thus, we want to find the condition in which

$$t(SSB, BE) = \frac{1}{2} t(DSB, BE), \tag{12}$$

where t is integration time and the notation "BE" means "break even". From the radiometer equation,

$$t = \frac{1}{\beta} \left[\frac{KT_{sys}}{T_{rms}} \right]^2, \tag{13}$$

where K is a constant determined by the switching mode and spectrometer efficiency, T_{rms} is the rms noise of the spectrum, and β is the bandwidth. Hence, we want to find the condition in which

$$T_{sys}(SSB, BE) = \frac{1}{\sqrt{2}} T_{sys}(DSB, BE). \tag{14}$$

From Equations 8 and 10, we find that

$$\begin{aligned} \frac{T_{sys}(DSB, BE)}{T_{sys}(SSB, BE)} &= \frac{2T_{rx}(DSB, BE) + 2T_A(sky)}{2T_{rx}(DSB, BE) + T_A(sky) + T_{image}} && (15) \\ &= \sqrt{2} && (16) \end{aligned}$$

Solving for $T_{rx}(DSB, BE)$ yields

$$T_{rx}(DSB, BE) = \frac{1}{\sqrt{2}} \left[T_A(sky) - \frac{T_{image}}{\sqrt{2} - 1} \right]. \tag{17}$$

Thus, if the DSB receiver temperature is below this break-even point, T_{sys} is dominated by sky noise and it is always more efficient to observe SSB.

This relation can also be expressed usefully in terms of the break-even sky noise, *i.e.,* if sky noise exceeds this value, you could make two SSB observations in less time than one simultaneous DSB observation with lines in both sidebands:

$$T_A(sky, BE) = \sqrt{2} T_{rx}(DSB) + \frac{T_{image}}{\sqrt{2} - 1}. \tag{18}$$

In practical cases, even if the SSB noise exceeds the break-even point, DSB observing may not be the most efficient mode if a choice between SSB and DSB observing is available. It will usually be the case that the lines in the two sidebands are not of the same strength or may not be of the same importance to the observer. Hence, integration times and signal-to-noise ratios may get skewed in a less than optimum way – *i.e.,* too much signal-to-noise in one sideband or not enough in the other. It will usually not be the case that DSB observing gives twice as much information as SSB. On the other hand, there are cases in which maximizing signal-to-noise is not as critical as minimizing observing overhead. DSB observing may be very useful in that case. There may be other cases in which having lines in both sidebands provides a useful system check or improves relative calibration.

In MMA Memo 70, Kerr outlined three options for sideband separation and/or rejection. Most current SSB systems use either quasi-optical filters or reactive termination in the mixer block using mechanical backshorts. Neither of these options would seem practical for the number of receivers in the MMA. If the RF performance can be achieved, image rejection mixers (MMA Memo 151; Kerr & Pan) would be more practical from an operations and reliability standpoint. In principle, such systems provide the ideal situation in which the information from both sidebands can be retained and analyzed separately, while the noise from the opposite sideband is rejected. Analyzing both sidebands independently would require doubling the size of the MMA correlator and may not be practical. The technique can probably be implemented at many single-dish facilities without requiring additional backend hardware.

4 Receiver Performance Goals

As receiver temperatures get better, we may reach a point in which atmospheric and spillover noise dominate system noise such that further reductions in receiver noise result in insignificant improvements in sensitivity. In terms of the equations presented above, we can prescribe a practical performance goal, at least parametrically. The DSB noise temperature of the ultimate receiver when using the Planck equation to express physical temperatures as equivalent radiation temperatures is given by Kerr, Feldman, and Pan in MMA Memo 161 as

$$T_u = \frac{h\nu}{2k} \tag{19}$$

The question is how close do we need to get to this limit before further improvements are insignificant in terms of integration time. To parameterize the problem, let us define an "acceptable" integration time (t_a) representing the time necessary to achieve an arbitrary sensitivity and define an "ultimate" integration time required for a quantum-limited receiver (t_u), but in the presence of atmospheric and spillover noise. Let "n" be the performance degradation we consider acceptable. An appropriate value for this factor might be 2.

From the system temperature equation (Equation 1) and the radiometer equation (Equation 13),

$$\frac{t_a}{t_u} = \left[\frac{2T_{rx}(DSB) + T_A(sky) + T_{image}}{2T_u + T_A(sky) + T_{image}}\right]^2 \tag{20}$$

$$= n \tag{21}$$

where we are assuming that the observation is made in SSB mode but that T_{rx} is a DSB receiver noise temperature. Solving for $T_{rx}(DSB)$, we find

$$T_{rx}(DSB, acceptable) = \sqrt{n}T_u + \left(\frac{\sqrt{n}-1}{2}\right)(T_A(sky) + T_{image}). \tag{22}$$

5 The Dual-Polarization Advantage

Although we assume this is widely recognized, we note here that the best way to improve system performance at a given site with a given telescope and receiver system is to have orthogonal polarization channels. Dual polarizations of equal sensitivity always reduce observing time by a factor of 2 regardless of observing conditions. Doing SSB rather than DSB measurements offers this much improvement only at large values of sky noise.

6 SSB versus DSB Performance Comparisons using MMA Parameters

The design specifications for the MMA call for an antenna with as little as 2% loss to rear spillover, blockage, and ohmic heating (η_l). This leads to quite small spillover noise. Furthermore, the sites being examined have very low precipitable water vapor and high transparencies. Atmospheric and antenna spillover noise are thus lower for the MMA than for many existing mm/submm telescopes. Consequently, the suppression of image noise is less important at the lower frequencies and under the best skies. On the other hand, if the image separating mixer scheme is successful, the effective termination temperature of the image is quite low and can still lead to a noise advantage for SSB systems.

For our calculations, we have used these parameters:

$\eta_l = 0.98$

$\eta_{fss} = 0.73$ (divides out in Tsys ratios)

PWV = 1 mm

$T_{amb} = -5$ C

Elevation angle = 45 deg

$\frac{T_{spill}}{T_{amb}} = 0.95$

$\frac{T_{atm}}{T_{amb}} = 0.95$

$T_{rx}(DSB) = 4\left(\frac{h\nu}{2k}\right)$

$T_{image} = 4.2$ K

Atmospheric opacities were produced by the Grossman (1989) model. When using these calculated atmospheric opacities, we have ignored any differences between the atmospheric opacities in the signal and image sidebands. Note that near the atmospheric band edges, this assumption will break down.

Figure 1 shows $T_{sys}(SSB)$, $T_{sys}(DSB)$, and Γ (the DSB penalty) as a function of τ_0 for two sets of image termination conditions. The first termination condition is a traditional cold-load termination such as is achieved in current quasi-optical rejection schemes which give $T_{image} \simeq 30$ K. The second condition is appropriate to a sideband separating mixer system for which $T_{image} = 4.2$ K. For $\tau_0 < 0.1$, and $T_{image} = 30$ K, the DSB system temperature is less than than the SSB system temperature (*i.e.,* Γ is negative). For $T_{image} = 4.2$ K, $T_{sys}(DSB)$ is never less than $T_{sys}(SSB)$, pointing to the importance of achieving low termination temperatures.

We also show in Figure 1 the sky temperature $T_A(sky)$ and the two dominant terms which contribute to $T_A(sky)$ (T_{ant} and T_{sky}; T_{cmbr} is always less than 0.2 K at this frequency). A significant contribution to the system temperature is that due to rear spillover noise, which points to the importance of designing antenna structures and optics to minimize rear spillover and blockage losses. Finally, in Figure 1 we show a comparison between the quantities $T_{rx}(DSB, BE)$ (Equation 17) and $T_{rx}(DSB, acceptable)$ (Equation 22). If receiver temperatures are below this break-even point, sky noise dominates and SSB observations are always more efficient even if astronomical measurements can be collected from both sidebands.

Figure 2 shows the Chilean MMA site atmospheric opacity as a function of frequency calculated using the Grossman (1989) atmospheric model. Figure 3 shows the differences between single and double sideband system temperatures as a function of frequency for typical atmospheric conditions at the proposed Chilean MMA site. We have assumed the telescope parameters listed above and an image termination temperature of 4.2 K.

Figure 4 shows the squared ratio of the DSB and SSB system temperatures and thus gives the observing speed ratio for the two options. In the high-transparency 200-300 GHz window, the observing time advantage of SSB is only 25-30%. At higher frequencies for which transparency diminishes and noise climbs, the SSB advantage grows. For the submillimeter windows above 400 GHz, the SSB advantage is over a factor of 2. This implies that one could do two SSB observations faster than one DSB observations even if the lines of interest could have been observed simultaneously in opposite sidebands.

These results are for good observing conditions (PWV = 1 mm) and assumes that the high rear spillover efficiency ($\eta_l = 0.98$) can be realized. As the weather deteriorates, the SSB advantage grows. Similarly, if η_l is less than assumed, the SSB advantage grows. Figure 5 shows how the squared ratio of the DSB and SSB system temperatures depends on τ at 230 GHz. The squared Tsys ratio is a rather steep function of opacity at low values of τ. Thus, as the weather becomes marginal or if you are observing at low elevation angles, SSB-mode observing will offer significant sensitivity advantages over DSB-mode observing.

Figure 6 shows the dependence of $T_{rx}(DSB, acceptable)$ (Equation 22) with frequency for the conditions shown. The Grossman (1989) atmospheric model was used to calculate the atmospheric contributions to $T_A(sky)$. Shown with $T_{rx}(DSB, acceptable)$ is the ultimate DSB receiver temperature, T_u. Note that $T_{rx}(DSB, acceptable) > T_u$ at all frequencies for the conditions shown, using $n = 2$. Below 400 GHz, an acceptable receiver temperature (within a factor of 2 of the theoretical limit in integration time), is about 2 times the quantum limit. At higher frequencies, it is 3-4 times the quantum limit owing to the greater sky noise.

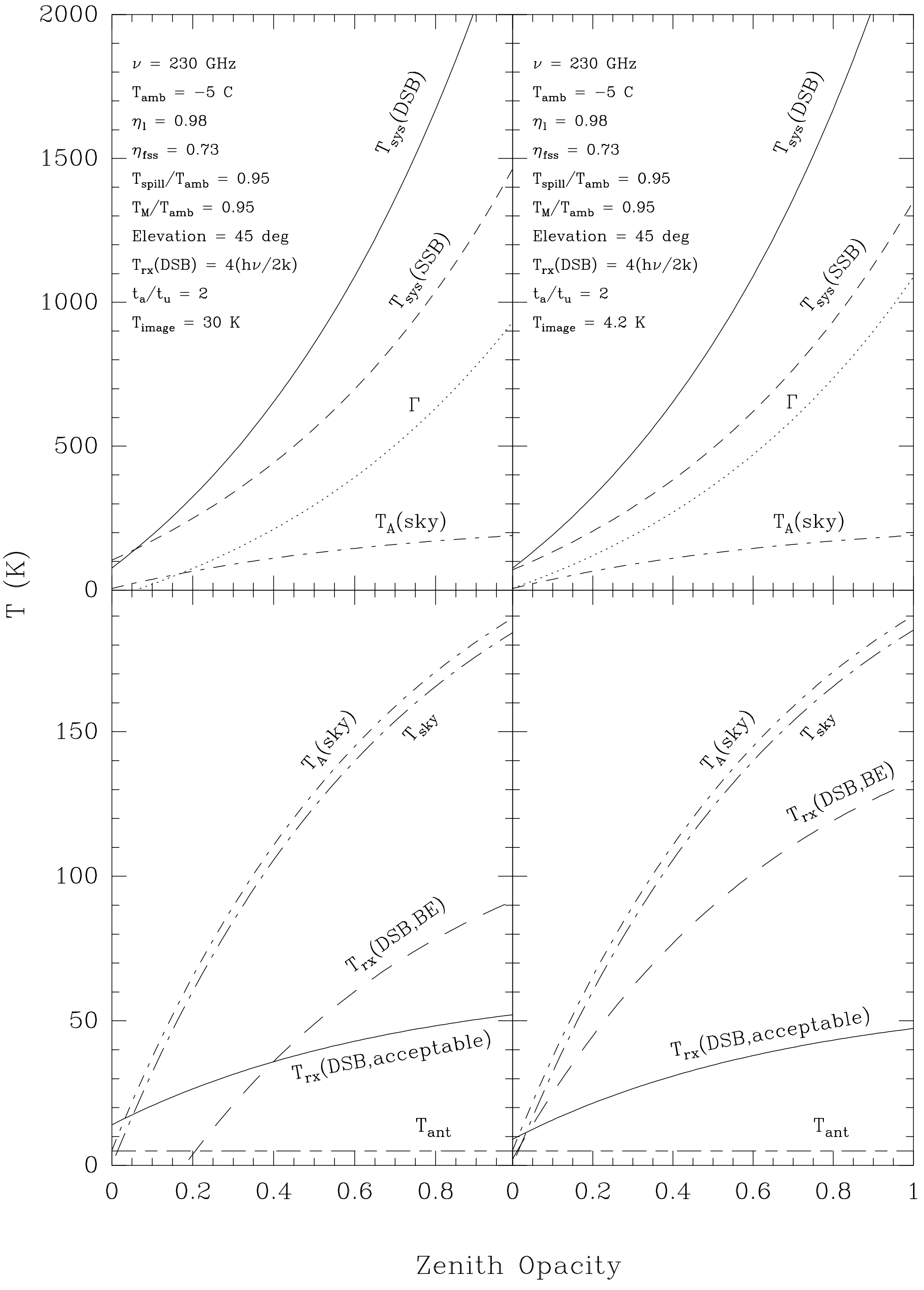

Figure 1: Representative receiver and system temperatures as a function of τ at 230 GHz. An image termination noise temperature of 30 K is representative of the traditional cold load termination technique used at the 12m. An image termination noise temperature of 4.2 K represents that expected from the image separating mixer at a physical temperature of 4.2 K.

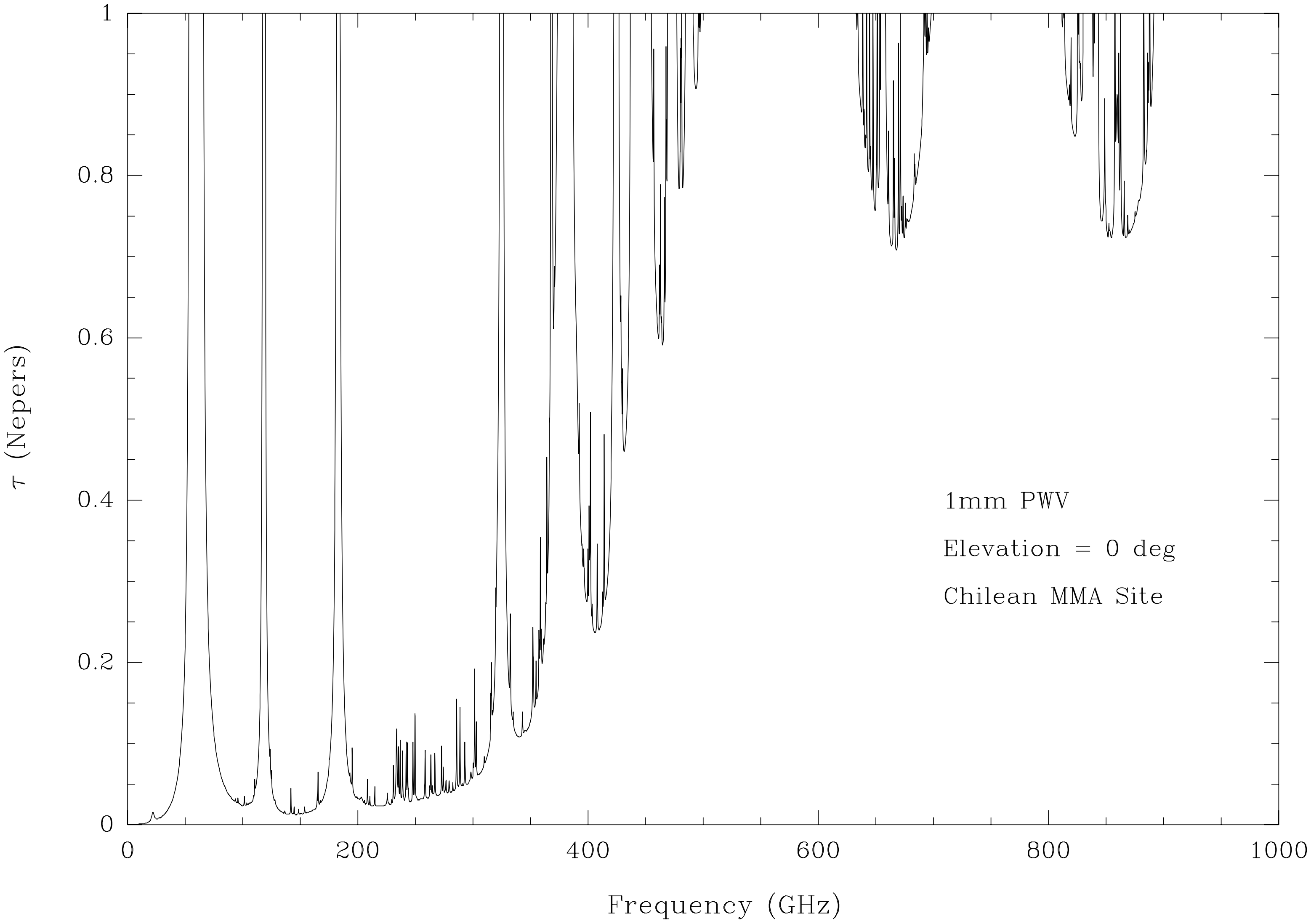

Figure 2: τ as a function of frequency for the Chilean MMA site. Calculated using the Grossman (1989) atmospheric model.

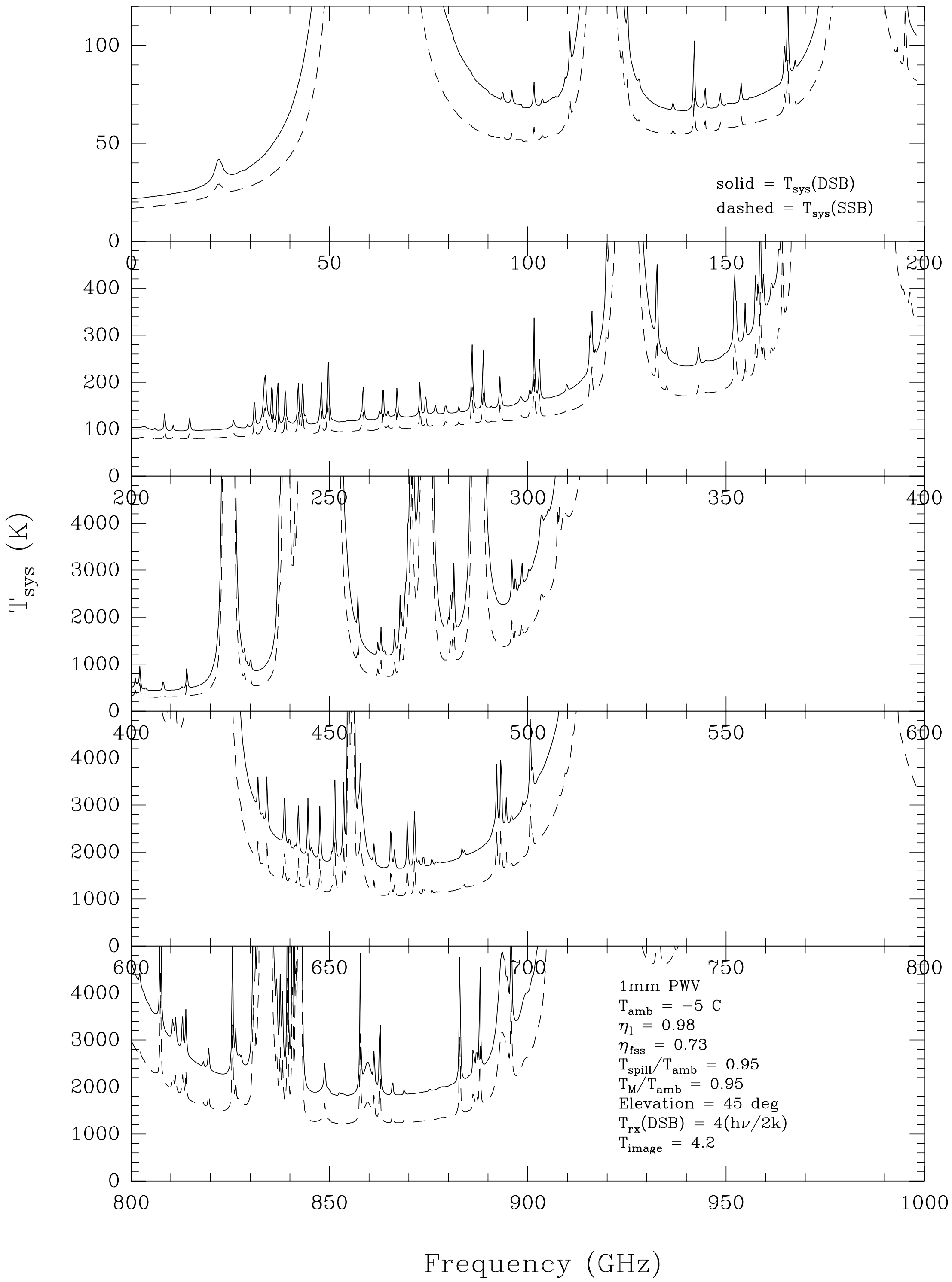

Figure 3: Single and double sideband system temperatures (T_R^* scale) as a function of frequency for the Chilean MMA site and the conditions shown in the lower right.

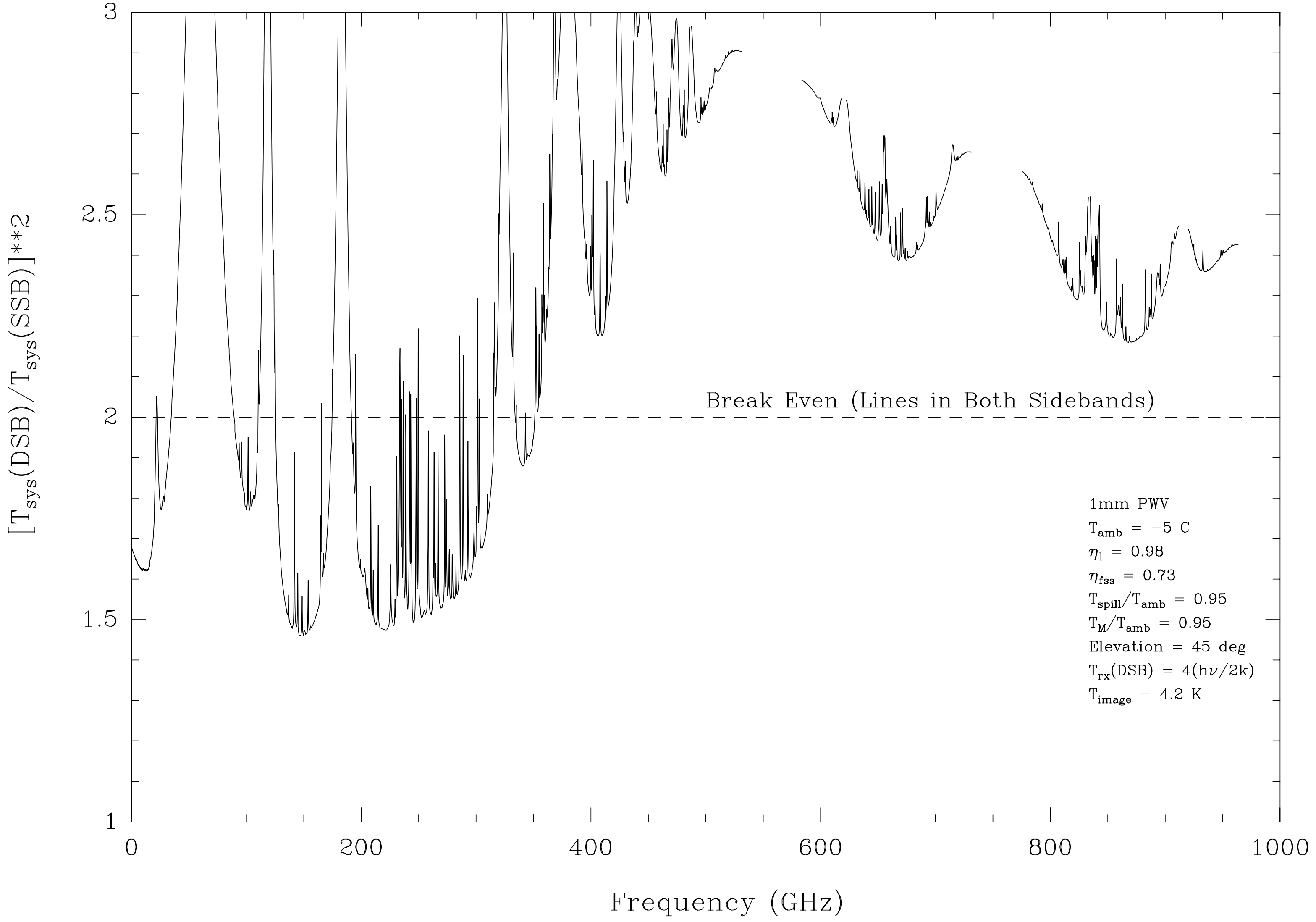

Figure 4: System temperature ratio as a function of frequency for the Chilean MMA site and the indicated conditions.

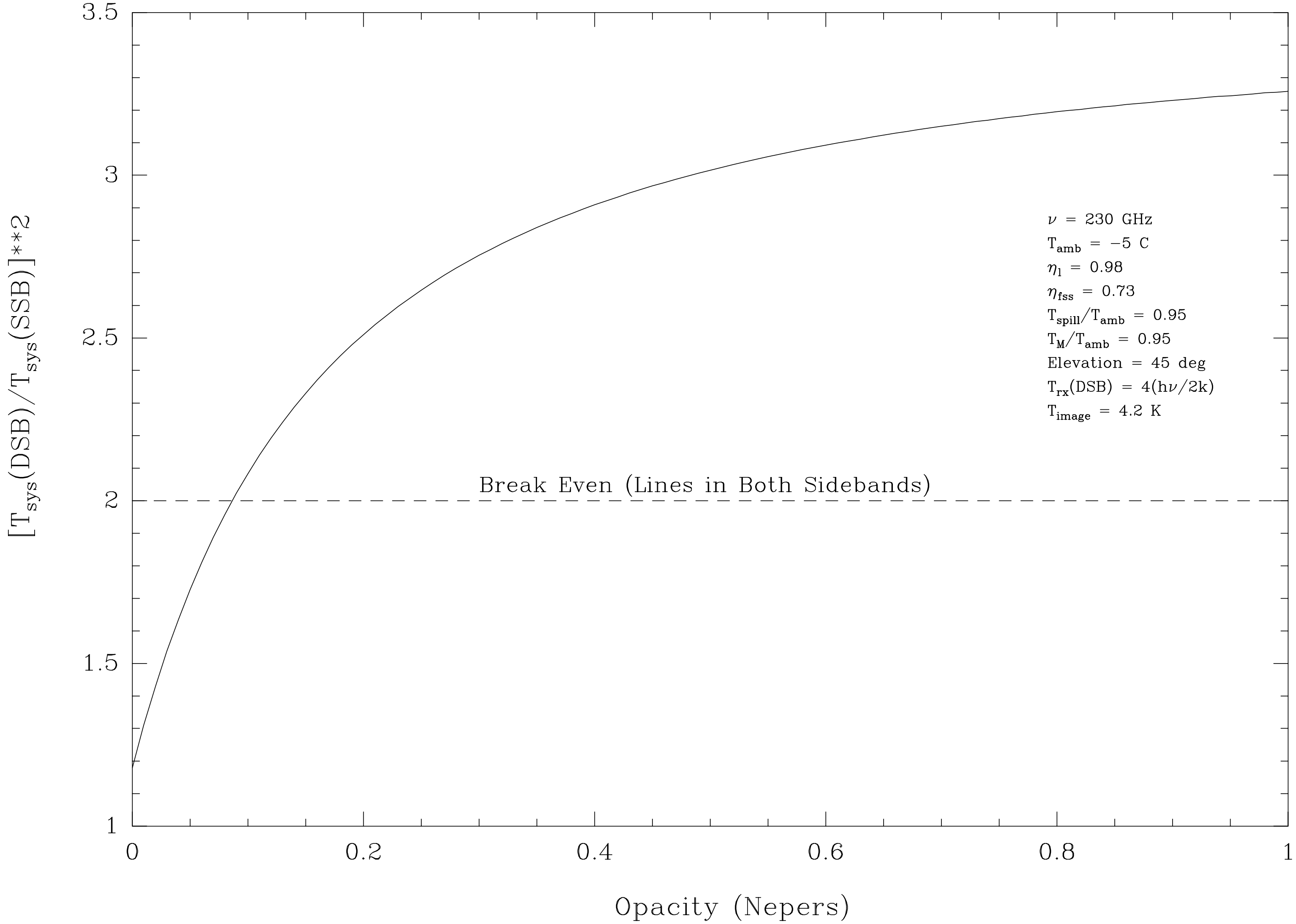

Figure 5: System temperature ratio as a function of τ for the indicated conditions.

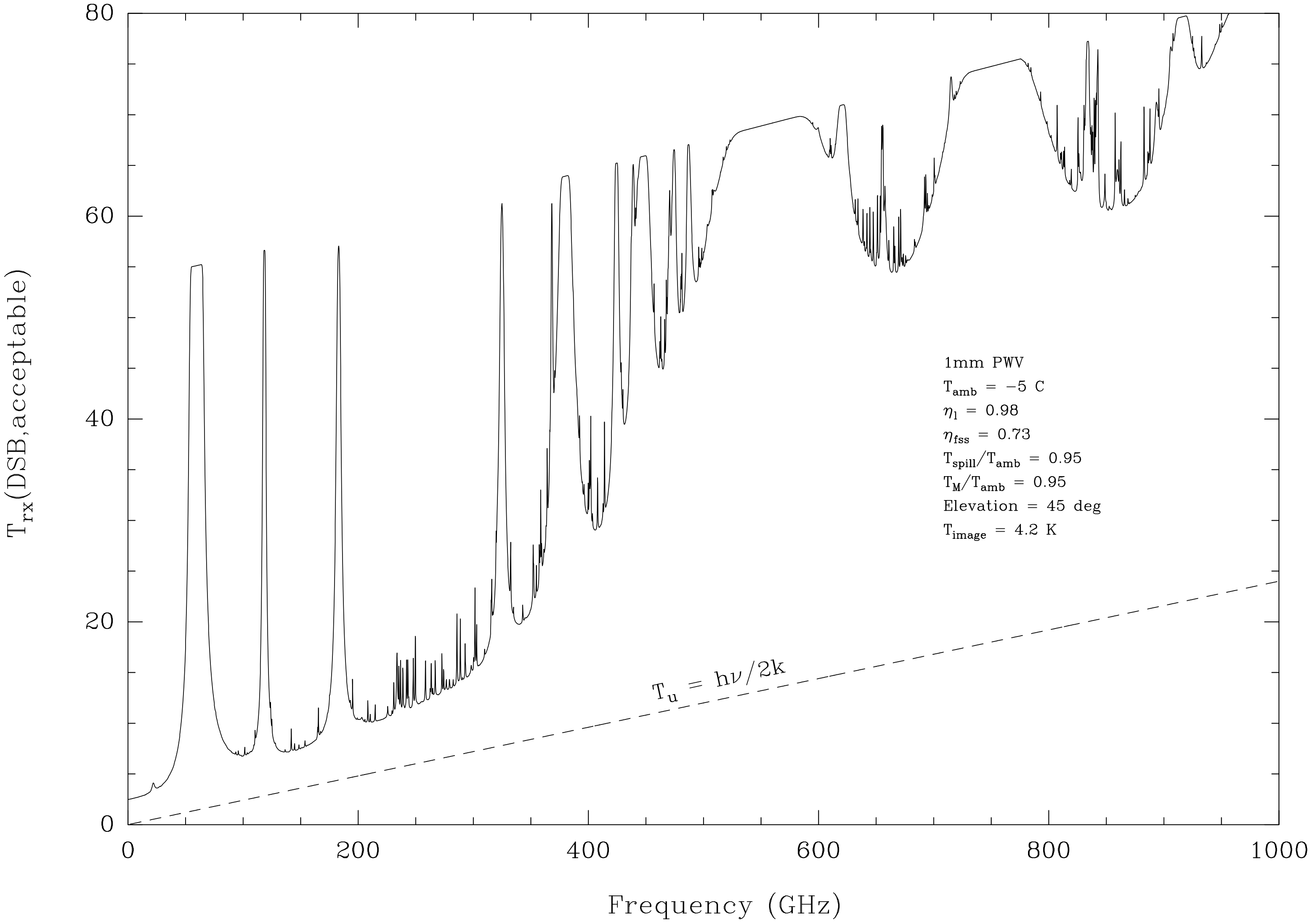

Figure 6: $T_{rx}(DSB, acceptable)$ as a function of frequency for the Chilean MMA site and the indicated conditions. The ultimate receiver performance T_u is also shown.

7 Whither Single or Double Sideband for the MMA?

For single dish observers, single sideband systems offer three main advantages: (a) rejection of image noise from the atmosphere and antenna; (b) improved calibration as the response to broadband calibration loads and the atmosphere is through only one sideband; (c) reduction of spectral confusion by image sideband lines. Millimeter-wave interferometers use phase switching techniques to separate the signal and image sideband responses. This eliminates the problems presented by item (c) above. The MMA is meant to operate in both interferometric and total power, single dish modes, however. The problems of spectral line confusion can be particularly onerous to many single dish Galactic spectroscopy projects. The motivation for SSB systems are substantial on these grounds alone.

The issue is less clear concerning atmospheric and antenna noise effects and depends rather critically on the particular observing frequency and water vapor conditions. In the 1.3 mm (230 GHz) band under excellent sky conditions (1 mm PWV), an SSB system offers ~50% improvement in observing speed over a DSB system. This difference increases to greater than 85% at 345 GHz. Above 400 GHz, the difference in observing speed is over a factor of 2. If atmospheric conditions deteriorate or if the antennas do not have such low spillover losses as specified, the advantage of SSB operation is larger.

Below 300 GHz, noise reduction alone is perhaps not a compelling case for SSB operation. Nevertheless, we conclude that because of single-dish mode observing and because of noise reduction above 300 GHz, SSB capability is worth substantial technical development effort.

8 Continuum Measurements

In the above we have concentrated on how SSB and DSB observing affects spectral line observations. For continuum measurements, DSB observations double the detection bandwidth. With 16 GHz of bandwidth, a doubling of the bandwidth may not be desirable. The 460-490 GHz, 660-690 GHz, and 820-900 GHz atmospheric windows are much narrower than the lower-frequency wavebands and contain strong absorption lines due to telluric O_2 and H_2O. These intrusions will make placement of the full 16 GHz of bandwidth difficult.

It would seem that the image-separating mixer would be an ideal design which would meet the needs of both spectral line and continuum observers.

Continuum observers could take advantage of the dual-sideband capabilities, while spectral line observations would benefit from the ability to reject the image sideband.

9 Conclusions

1. We demonstrate that with respect to the signal sideband, DSB observations are noisier than SSB observations by the term (Equation 11)

$$\Gamma = \frac{T_A(sky) - T_{image}}{\eta_l \eta_{fss} \exp(-A\tau_0)}$$

2. Using DSB systems, spectroscopists often analyze lines in both sidebands. Above certain levels of antenna and atmospheric noise, it may be more efficient to perform two SSB observations rather than one simultaneous DSB observation if SSB capability is available. In terms of receiver temperature, we show that the break-even point is given by (Equation 17)

$$T_{rx}(DSB, BE) = \frac{1}{\sqrt{2}}\left[T_A(sky) - \frac{T_{image}}{\sqrt{2}-1}\right].$$

   Below this receiver temperature, sky and antenna noise dominate and SSB mode is always more efficient.

3. Receiver noise temperatures are improving year-by-year and some devices are already within a factor of a few of the quantum noise limit. Because of the presence of atmospheric and antenna noise, we may soon reach the point of diminishing returns in further lowering receiver noise temperature. Parametrically, we show that the acceptable lower limit for receiver DSB noise temperature can be written as (Equation 22)

$$T_{rx}(DSB, acceptable) = \sqrt{n}T_u + \left(\frac{\sqrt{n}-1}{2}\right)(T_A(sky) + T_{image}).$$

where n is the degradation factor in observing speed that we are willing to tolerate over a quantum-limited receiver. An appropriate choice for n might be 2. In the 230 GHz band, the "acceptable Trx" is about twice the quantum limit; in the 650 GHz band, it is about 3.6 times the quantum limit.

4. We emphasize that keeping antenna spillover losses to a minimum pays large dividends for any system and that keeping the image termination temperature as low as possible is critical for SSB systems. We also emphasize that among ways to achieve lower noise, a dual polarization system usually leads to the most improvement.

5. We show that for the anticipated MMA antenna parameters and atmospheric transparencies appropriate to good weather on the Chilean or Mauna Kea sites, SSB systems offer observing speed improvements over DSB systems of $\sim$50% at 230 GHz, >85% at 345 GHz, and over a factor of 2 above 400 GHz.

6. We note that for single-dish mode, which the MMA is also intended to support, SSB systems are often important for improving calibration and reducing spectral confusion from the image sideband. The latter point is not an issue in interferometer mode as the sidebands can be separated by phase switching.

7. Below 300 GHz, the noise advantage of SSB systems is perhaps marginal, at least under the best skies and assuming that the specified antenna performance is achieved. However, the DSB-to-SSB integration time ratio is a steeply rising function at low opacity. Thus, if weather conditions deteriorate even slightly, the SSB advantage grows rapidly. Above 300 GHz, the noise advantage of SSB-mode observing is almost always significant.

8. Given the advantage to single dish observing and the noise improvement above 300 GHz, we conclude that development work to achieve a SSB capability for the MMA is well-justified.

10 References

Callen, H. B. & Welton, T. A. 1951, Phys. Rev., 83, 34.
Grossman, E. 1989, Atmospheric Transmission Software, version 1.5.
Kerr, A. R., MMA Memo 70.

Kerr, A. R. & Pan, S.-K., MMA Memo 151.
Kerr, A. R., Feldman, M. J., & Pan, S.-K., MMA Memo 161.
Kutner, M. L. & Ulich, B. L. 1981, ApJ, 250, 341.
Ulich, B. L, & Haas, R. W. 1976, ApJS, 30, 247.